

Unravelling the role of architecture in polymer-based glues for hydrogels

Kaiye Xie,[†] Nicola Molinari,[‡] Chengcheng Xiao,[†] and Stefano Angioletti-Uberti^{*,†}

[†]*Department of Materials, Imperial College London, London, UK*

[‡]*John A. Paulson School of Engineering and Applied Sciences, Harvard University,
Cambridge, MA 02138, USA*

E-mail: sangiole@imperial.ac.uk

Abstract

We investigate polymers of different architectures as potential candidates for the development of glues for hydrogels. By using a combination of coarse-grained modelling and molecular dynamics simulations, we systematically characterize the link between experimentally tuneable parameters and adhesion energy. We find that, for a broad set of parameters, adhesion is controlled almost exclusively by the total amount of glue at the interface as well as by the glue-hydrogel affinity. Instead, it is largely independent of changes in polymer architecture as well as size, a conclusion that shines new light on previously observed experimental trends. Additionally, we show that the scaling behaviour of the properties we measure can be explained by modelling the glue as an ensemble of ideal, non-interacting, linear polymer segments. We expect that the fundamental insights herein provided will aid the design of new polymer-based adhesives for hydrogels.

Introduction


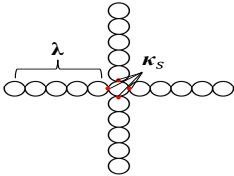
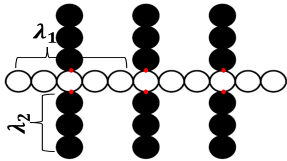
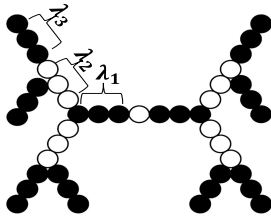
Adhesives have been used by mankind for many centuries and underpin a large variety of technological applications in different fields, from manufacturing, where they can be used to glue different materials together,¹ to biomedical applications such as the development of glues for biological tissues for suture-less wound healing.²⁻⁴ Despite the fact that most adhesives are based on polymers, finding adhesives to stitch two polymers together still represents an important technological challenge. This is particularly true in the case of hydrogels, i.e., water-swollen polymer networks.^{5,6}

Because of their biocompatibility, mechanical properties and ability to respond to different stimuli, hydrogels represent a particularly important class of biomaterials.⁷ In fact, the so-called extra cellular matrix, one of the main components of most biological tissues, is itself an hydrogel.⁸ For this reason, glues for hydrogels have received particular attention, not only in academia and industry but also in the popular press. In fact, these type of glues are sometimes emphatically named “glues for organs” to highlight their potential to repair wounds, much in the same way that we use glues to re-attach common broken items. In this regard, a large variety of systems have been presented as potential candidates.^{2,3,9} Li *et al* have first shown that mussel-inspired binding agents can be combined with a dissipative matrix to form so-called tough adhesives that can reliably attach hydrogels together with large adhesion energies, of the order of $1000 \text{ J} / \text{m}^2$.³ Such a high adhesion energy makes these glues ideal for applications where the bonded interfaces must be able to sustain large stresses without unbinding, e.g., when attachment to muscles such as the heart. Due to their high viscosity, however, tough adhesives do not easily spread on a surface, preventing their direct use as a glue during surgery where wounds must be quickly sealed.¹⁰ One way to overcome this problem is to use fast photo-curable adhesives that can be cross-linked and activated after deposition. For example, Lang *et al* developed a solution of poly(glycerol sebacate acrylate) (PGSA), a highly biocompatible polymer, mixed with a photoinitiator that could

be used to cross link the polymer together using UV light within seconds of exposure.¹¹ In this case, the system was shown to easily spread on a surface before cross-linking, facilitating its application *in situ*. Despite this advantage, the need for UV-light exposure and the potential collateral damage this can induce to peripheral tissue can limit its use in clinical settings. A different solution to the problem of gluing hydrogels together has been proposed by Rose *et al*,² which showed that a solution of nanoparticles can act as an optimal glue. In this case, it is the polymer’s ability to form multiple yet reversible bonds with the surface of the nanoparticle that determines adhesion. The advantage of this solution is that such glues can be directly and easily “painted with a brush” on the tissue in question, thanks to their low viscosity. However, the adhesion strength offered by this system is about two orders of magnitude smaller than those offered by tough adhesives,^{2,3} which limits their range of application especially when large stresses have to be sustained over prolonged time. Previously, we presented theoretical and simulation results that highlighted the relative influence of different parameters in determining nanoparticles-induced adhesion.^{12,13} In summary of our previous findings, the two main problems limiting adhesion were i) the presence of a critical concentration, due to packing constraints induced by excluded volume interactions, above which nanoparticles start to form inert layers that decrease adhesion and ii) only particles below a certain chemistry-dependent size can act as glues, whereas above this critical size the opposite effect is observed. Thus, non-optimised nanoparticles might not just have a sub-optimal performance, but instead even prevent adhesion rather than reinforcing it, acting as anti-adhesives surface passivators, or lubricants. In general, these phenomena depend on excluded volume effects that limit the concurrent presence of both nanoparticles and hydrogel at the interface, lowering the amount of bridging bonds that can be formed and thus limiting the maximum adhesive performance of the glue. One potential way to overcome the drawbacks implicit in the use of inorganic, hard nanoparticles would be to use what are sometimes and improperly referred to as “soft” nanoparticles¹⁴ e.g., polymers with star-like, brush or dendritic architectures, see Table 1 for reference. **Note that we use**

the term architecture to refer to the way that branching leads to a deviation from a linear polymer chain.

Table 1: Schematic representation of the different polymer architectures and structural parameters described in this study. a) Linear polymers, the variable parameter is their length λ . b) Star polymers, where the two parameters are the number of arms κ_s and the length of each arm λ (In this sense, a linear polymer can be regarded as a star polymer with $\kappa_s = 2$. In this work 3, 4, 6-arm star polymers are investigated c) Brush polymers, where the structural parameters are the length of the backbone λ_1 (white spheres), the length of each side arms λ_2 (black spheres) and their numbers κ_s . d) Dendrimers, for which the parameters investigated have been the number of generations g . For instance, the schematics show a 3rd generation dendrimer, where different generations are distinguished by different colors. Besides, the length of each arm within two branching points and the number of arms at each branching point are variables.

Architecture	(a) Linear 	(b) Star 
Parameters	λ : Length of arm	λ : Length of arm κ_s : No. of arms
Architecture	(c) Brush 	(d) Dendrimer 
Parameters	λ_1 : Length of backbone λ_2 : Length of side arm κ_s : No. of side arms	λ_1 : Length of 1 st generation λ_2 : Length of 2 nd generation λ_n : Length of n^{th} generation

In this regard, we point out that what we do not include in this category nanoparticles made of highly cross-linked polymers, such as those studied by Arno *et al.*¹⁵ These type

of particles are more similar to hard, inorganic nanoparticles in that once in contact they strongly repel each other. Instead, in the architectures we consider here the effective repulsion is very weak,¹⁶ in some cases even finite and of the order of the thermal energy.¹⁷ We hypothesise that this difference between hard-core and soft-core repulsion should allow for a different packing of the glue at the interface, and qualitatively change its behaviour. At the same time, the total contact area for these soft nanoparticles grows faster than $V^{2/3}$ (V being the particle's volume). For a fixed amount of glue, this scaling behaviour of the contact area should allow to establish a larger number of attractive interactions with the gel compared to hard nanoparticles, increasing their gluing performance.

Based on the aforementioned premises, we use coarse-grained modelling and Molecular Dynamics (MD) simulations to investigate the link between the polymeric architecture of these soft nanoparticle, which we will refer to also as the gluing polymer, and their ability to glue swollen hydrogels' interfaces together. The remainder of our paper is organised as follows. In the next section, we provide the details of our coarse-grained model as well as of the molecular dynamics simulations we performed. Then we present and discuss our results, and rationalise these results based on the underlying microscopic picture arising from the simulations, while also providing a simple physical model able to qualitatively capture the observed behaviour. We later discuss the connection between our observations and existing experimental data, and how our simulation results could translate to design rules for glues based on these polymer architectures. In the final section, we summarize our results and provide an outlook on potentially interesting new avenues for future research.

Modelling details

Our modelling strategy closely follows our previous works on nanoparticle-based glues for hydrogels and other cross-linked polymer networks,^{12,13,18} which proved to be successful in capturing different experimental observations. Hence, we use a simple bead-spring repre-

sentation for both the gluing polymers and the hydrogel. In our system, the non-bonded interactions between any two beads are described via a simple Lennard-Jones (LJ) potential:

$$V_{LJ} = \begin{cases} 4\epsilon\left[\left(\frac{\sigma}{r}\right)^{12} - \left(\frac{\sigma}{r}\right)^6\right], & r \leq r_{\text{cut}} \\ 0, & \text{otherwise} \end{cases} \quad (1)$$

Where σ , ϵ and r_{cut} have the usual meaning in the context of Lennard-Jones potentials. For this reason, we also use Lennard-Jones reduced units throughout the manuscript, unless otherwise stated, a choice that makes all quantities dimensionless. **The Lennard-Jones potential, particularly in the truncated form employed here, is often used as the basis of coarse-grained models to describe non-covalent interactions in a variety of systems, from synthetic polymers to proteins or lipids.^{19,20} The reason for its widespread use is that the potential functional form allows to describe and tune in a relatively simple way, or even completely remove the influence of, two main characteristics present in most type of molecular interactions: excluded volume interactions and a finite-range attraction. Whereas this potential can be too simple to predict strongly chemistry-dependent effects quantitatively, it has nevertheless proved extremely useful at unravelling robust qualitative trends.²¹ A good recent paper reviewing the Lennard-Jones potential in coarse-grained simulations focusing on its use, and on when not to use it, can be found in Ref. 22.**

In order to describe their different physical behaviour, we use three independent sets of LJ parameters: one for the hydrogel-hydrogel (GG), one for the hydrogel-gluing polymer (GP) and one for the gluing polymer-gluing polymer (PP) interaction. For the description of hydrogel-hydrogel interactions, all the parameters are kept constant at $\epsilon_{GG} = 0.5$, $\sigma_{GG} = 1.0$, and $r_{\text{cut},GG} = 2.5$. We chose these values because, together with the specific value for the angular potential discussed later, they allow us to mimic a swollen gel, as we have shown in our previous work.¹³ Similarly, the gluing polymer to gluing polymer parameters are kept constant at $\epsilon_{PP} = 1.0$, $\sigma_{PP} = 1.0$, and $r_{\text{cut},PP} = 2^{1/6}$. This choice for $r_{\text{cut},PP}$

translates to a purely repulsive potential. The rationale for this choice is that the effective interaction between hydrophilic polymers, the main class of polymers used as glues for hydrogels, is expected to be repulsive.²³ This repulsion is a general phenomenon observed in hydrophilic systems²⁴ and typically explained as arising from the presence of a network of hydrogen bonds formed by the solvating water molecules around them. For two polymers to get in direct contact, this network must be either broken or distorted, causing an effective repulsive interaction as captured by our choice of potential. Finally, for the hydrogel-gluing polymer interaction we chose $\sigma_{GP} = 1.0$, $r_{\text{cut},GP} = 2.5$, and vary ϵ_{GP} between 1.0 and 5.0. This range allows us to simulate different degrees of attraction, or, in other words, different levels of affinity between the chemistry of the hydrogel and that of the glue. For clarity and to ease reproducibility, a full summary of all the parameters used for the non-bonding potential is presented in Table 2.

Table 2: Summary of Non-bonded Potential Parameters (Eq.1)

Type of Interaction	ϵ	σ	r_{cut}
Hydrogel to hydrogel (GG)	0.5	1.0	2.5σ
Hydrogel to gluing polymer (GP)	[1.0–5.0]	1.0	2.5σ
Gluing polymer to gluing polymer (PP)	1.0	1.0	$2^{1/6}\sigma$

The connectivity of the beads in both the hydrogel as well as within each gluing polymer is provided by a harmonic bonding potential between the beads of the form:

$$V_{\text{bond}} = \frac{1}{2}k_b(r - r_o)^2, \tag{2}$$

where $k_b = 80$, $r_o = 1.0$. As shown in previous work,¹⁸ this can provide stiffness to avoid high frequency modes and chain crossing. Because we are interested in simulating an hydrogel in the swollen state, we add among its beads an additional potential between triplets of bonded

neighbours, using again for simplicity an harmonic potential of the form:

$$V_{\text{angle}} = \frac{1}{2}k_a(\theta - \theta_0)^2 \quad (3)$$

where k_a , θ and θ_0 are the angular stiffness, the angle between every triplet and the equilibrium angle, respectively. All triplets have an equilibrium angle of $\theta_0 = \pi$, except the six non-collinear triplets involving a linker at junctions for which the equilibrium angle is $\theta_0 = \frac{\pi}{2}$. Note that this angular potential is only present between the beads of the hydrogel, but not those representing the gluing polymer.

Using the potentials discussed above, the hydrogel is represented as a regular network of beads, with cross-linking points equally spaced from each other to form a mesh size of 10 beads, see Fig.1 for clarity. The resulting cuboid hydrogel structure contains a total of 48500 beads arranged in 10 cells along the x and y direction, and 18 in the z direction (the straining direction). This system size was carefully chosen and verified to be sufficiently large to eliminate finite size effects. A cut is then introduced onto a plane parallel to the x-y plane to generate an interface between two cuboid hydrogels. The two hydrogels halves are then separated to form a gap to allow for the placement of the gluing polymers.

Once the hydrogel structures are generated following the above procedure, we perform MD runs to first equilibrate the hydrogel network alone, and then the whole system comprising the hydrogel and the gluing polymers. This two-step process is performed as follows. A gluing polymer solution is generated by placing polymers beads randomly with the required connectivity to generate the wanted architecture and later equilibrated at constant temperature and volume via short MD runs without the presence of the hydrogel. During this equilibration, the size of the simulation cell is chosen to be slightly smaller than the gap between the two hydrogel interfaces. Once equilibrated in this way, the polymer solution is inserted in this gap and the whole system is compressed using isothermal–isobaric ensemble simulations with constant uniaxial pressure ($p_{zz} = 0.1, p_{xx} = p_{yy} = 0.0$) along the z-axis.

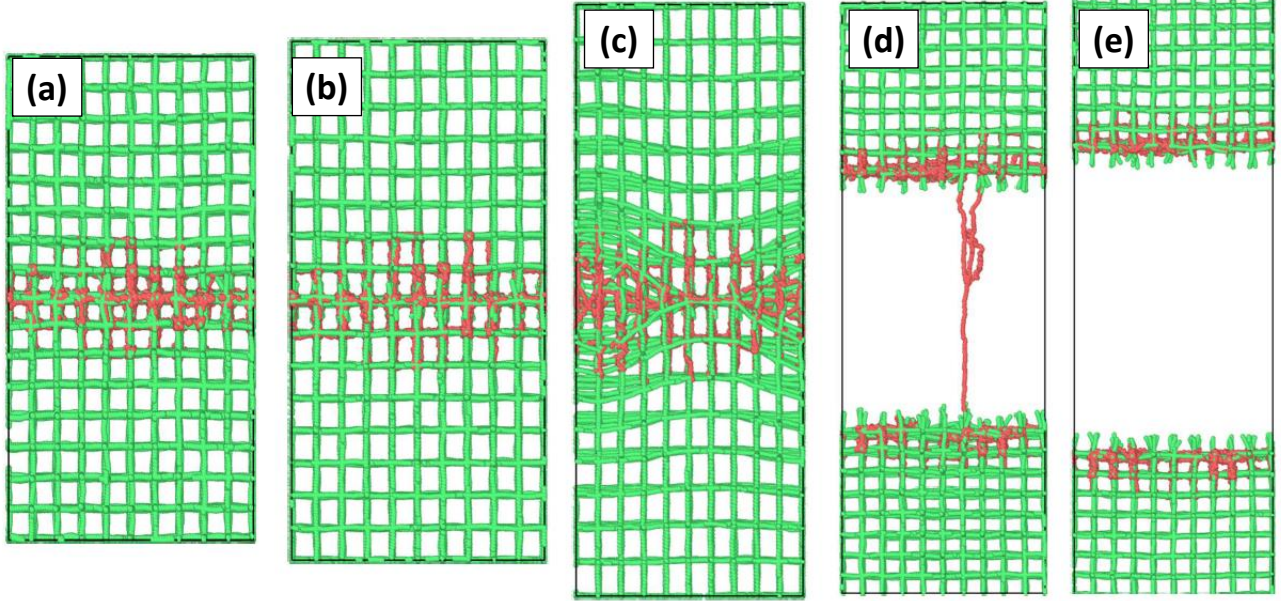


Figure 1: Representative snapshots of our system during the straining procedure. Red beads represent the gluing polymer and green beads the hydrogel. (a) In its equilibrated state without strain, the gluing polymers and the hydrogel are fully intertwined. (b-e) When uniaxial strain is gradually applied, at first the glue still binds the two stretching hydrogels together, but as tension increases, the elastic energy reaches a maximum, at which point it becomes favourable for the interfaces to separate, which require part of the glue to be pulled out (d). (e) Finally, the two hydrogels are completely separated, while the gluing polymers remain on their surface. Snapshots are created by using the visualisation software Ovito.²⁵

Finally, once the gap is fully closed, we remove the external pressure and further equilibrate the system under isostatic conditions at zero pressure. With the system prepared in this way, the final step which is equivalent to a tensile tests, is performed by elongating the simulation box along the direction perpendicular to the gel-gel interface (taken to be the z -direction) at a constant strain rate, while keeping the pressure along the x - and y -direction equal to zero. During this last step, the stress on the system against the deformation $\sigma_{zz} = -p_{zz}$ is recorded against the box elongation along the z -coordinate, providing a way to obtain stress-strain curves constituting the raw data from our simulation. For each set of parameters describing the system, we run five independent simulations. Results are reported as the average over these runs, with an error bar calculated as their root mean square deviation.

In all these steps, the temperature of the system is kept at $T = 1.0$. The temperature and pressure of the system are controlled via an MTK barostat-thermostat²⁶ and the equations

of motion are integrated using a velocity-Verlet algorithm with time step $\Delta t = 10^{-3}$ (in the proper LJ units). Finally, it should be noted that in all steps we apply periodic boundary conditions via the minimum image convention in all three directions, which allows us to simulate bulk gels. All simulations are executed using the HOOMD-blue MD software package^{27,28} on GPU. For clarity and reproducibility, the exact conditions used during each equilibration and pulling step are summarised in Table S1 in the supplementary information.

Results and Discussion

The stress-strain curves generated from our MD simulations are integrated up to the failure point to calculate the interface toughness, which we define as:

$$T = L_0 \int_0^{\bar{s}_{\max}} \bar{\sigma}_{zz}(\bar{s}) d\bar{s}, \quad (4)$$

where $\bar{\sigma}_{zz}$ is the zz component of the stress tensor (z being the straining direction), $\bar{s} = L_z/L_{z,0}$ is the strain in the simulation box along z (and \bar{s}_{\max} its maximum value at rupture). $L_{z,0}$ is the initial length along the z -axis of the simulation box at equilibrium and L_z its value during the straining procedure. In our simulations, pulling of the interface is performed at a rate, which we have checked is a sufficiently low value to maintain the system in quasi-static conditions, i.e. the measured stress-strain curve is independent on the applied strain rate for lower values. Under this condition, the measured toughness is equivalent to the free-energy density of adhesion $T \equiv \Delta F_{\text{adhesion}}$, i.e. the free-energy per unit area required to form two separated gels. The $\Delta F_{\text{adhesion}}$ for this system could have also been measured via more complex free-energy calculation techniques, see e.g. Refs.^{29,30}

In Table 1, we present schematically all the different polymer architectures we have studied here, for a total of more than 200 different combinations of structural parameters.

Specifically, we have studied four different polymer architectures: linear, star, brush and dendrimers. In panel b), for star polymers, changes in the structural parameters involved the number of arms κ_s and the length of each arm λ_s . Note that the case $\kappa_s = 2$ correspond to a linear polymer, panel a), with total length $2\lambda_s$. We investigate 3,4 and 6 arm star polymers with arm length between 30 to 60 beads. Similarly, for brush polymers, panel c), we investigate the effect of varying either the number of side arms $\kappa_{bb,s}$, their length $\lambda_{bb,s}$ as well as the length of the backbone $\lambda_{bb,b}$. Finally, for dendrimers, panel d), we study the effect of varying the number of generation g , the length of each generation λ_d and the number of arms per each generation κ_d . Mainly 5th and 6th generation dendrimers are tested. Finally, we also randomly mix different structures together, which we later refer to as the random mixture.

In Fig.2 we summarize the adhesion energy $\Delta F_{\text{adhesion}}$. This quantity is reported as a function of the total amount of glue inserted at the interface per unit area, as measured by the surface density of gluing polymer beads $\rho = N_{\text{beads}}/A$, where N_{beads} is the total number of beads, and A is the cross-sectional area of the simulation box. In practice, this density is proportional to the weight percent of glue at the interface often used as the control parameter in experiments, see e.g.¹⁵ For a single panel, different data points correspond to polymers of different architecture (represented with different point styles), same architecture but different values for the structural parameters (see Table 1 for reference) or same architecture and structural parameters but different concentrations. In the mean time, different colours correspond to different values of the glue-network affinity, as measured by the parameter ϵ_{GP} . Furthermore, for representative selected parameters values, Fig.3 shows the $\Delta F_{\text{adhesion}}$ as a function of the affinity ϵ_{GP} , for different architectures, considering a constant interface density for the representative case of $\rho_s = 0.7$. Together, Fig.2 and Fig.3 show the most important features of our system. The first feature we observe is that these soft-nanoparticles always improve adhesion, regardless of the value of their affinity. This is in

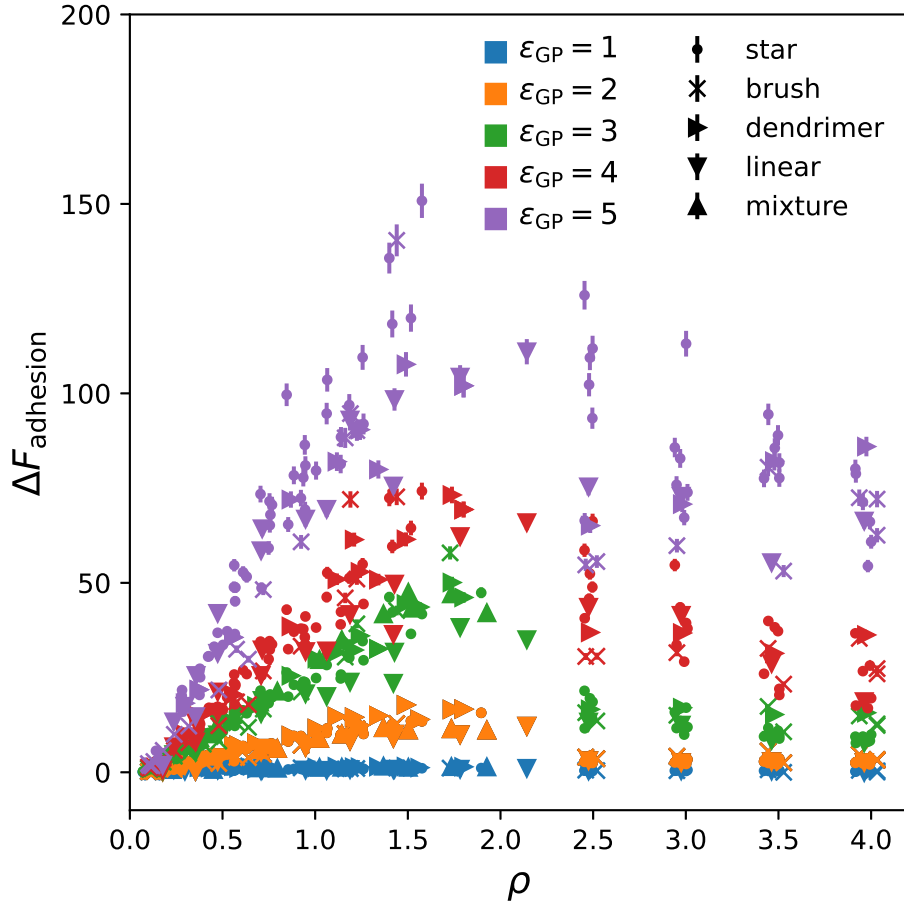


Figure 2: Adhesion free-energy $\Delta F_{\text{adhesion}}$ as a function of the amount of gluing polymer deposited at the interface, as measured by the density of gluing polymer beads ρ . Note that all quantities are reported in reduced Lennard-Jones units and are thus dimensionless. Different colors represent different gluing polymer - hydrogel affinities ϵ_{GP} , while the shape of the data points represent different architectures of the glue: star (dots), bottle-brush (crosses), dendrimers (right-pointing triangles), linear (bottom-pointing triangles) and a random mixture (top pointing triangles) of the four above. $\Delta F_{\text{adhesion}}$ is almost independent on the polymer architecture, and the different systems collapse into master curves that only depend on the glue-hydrogel affinity.

stark contrast with what has instead been observed in the case of hard nanoparticles-based glues.^{12,29,30} In this latter case, below a certain critical affinity the glue actually decreases the adhesion strength of the interface, effectively acting as an anti-adhesive. The second and somehow more unexpected feature we observe is that all the different systems roughly collapse on a master curve that, at least up to a surface densities of $\rho_s \approx 1.5$ where the maximum

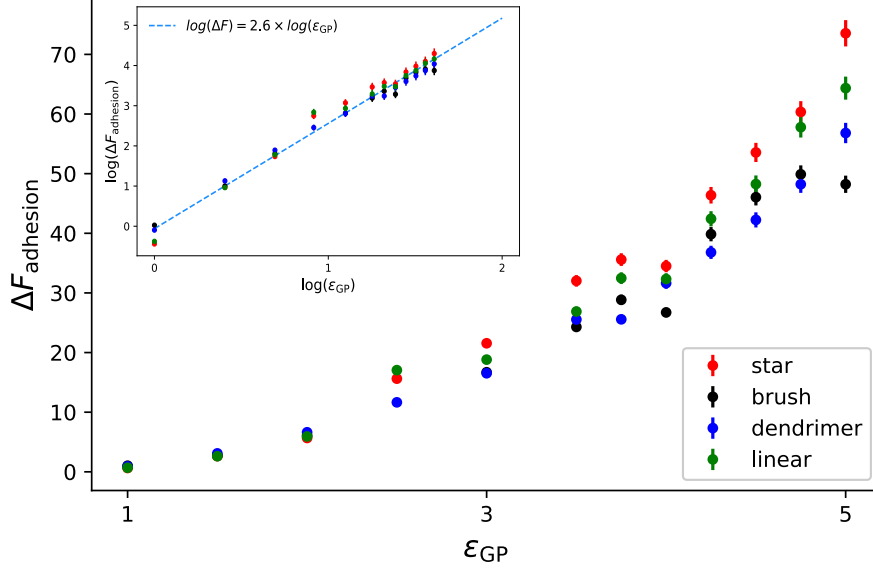


Figure 3: $\Delta F_{\text{adhesion}}$ as a function of gluing polymer - hydrogel affinity ϵ_{GP} , for different architectures at a representative surface density of glue $\rho = 0.7$. Inset: Same graph but plotted on a log-log scale. This last plot clearly shows a power-law behaviour, with a best-fit providing $\Delta F_{\text{adhesion}} \propto \epsilon_{\text{GP}}^{2.6}$. Note that all quantities are reported in reduced Lennard-Jones units.

adhesion is achieved, only depends on affinity (in Fig.2). In other words, these glues are indifferent to details such as the polymer architecture or the degree of polymerisation and its response only depends on the affinity of the glue for the hydrogel network and the total quantity of glue present at the interface. That adhesion is independent on the details of the system in this regime is also confirmed by a set of simulations (Fig.2, indicated as “mixture” in the legend), where instead of an homogeneous set of polymers of the same architecture and structural parameter, a random mixture of four types of structures is simulated. The system robustness to changes in architecture is more general and does not only apply to $\Delta F_{\text{adhesion}}$, but also to other quantities used to measure glues performance, such as the maximum stress and the maximum strain at failure, see Fig.4 (a) and (b) respectively.

In the following, we try to describe in more details the mechanism leading to the observed behaviour, and provide a qualitative explanation compatible with our observations. In doing that, we first notice that similar values for $\Delta F_{\text{adhesion}}$ for different architectures might arise from the averaging procedure that results from integrating potentially different stress-strain

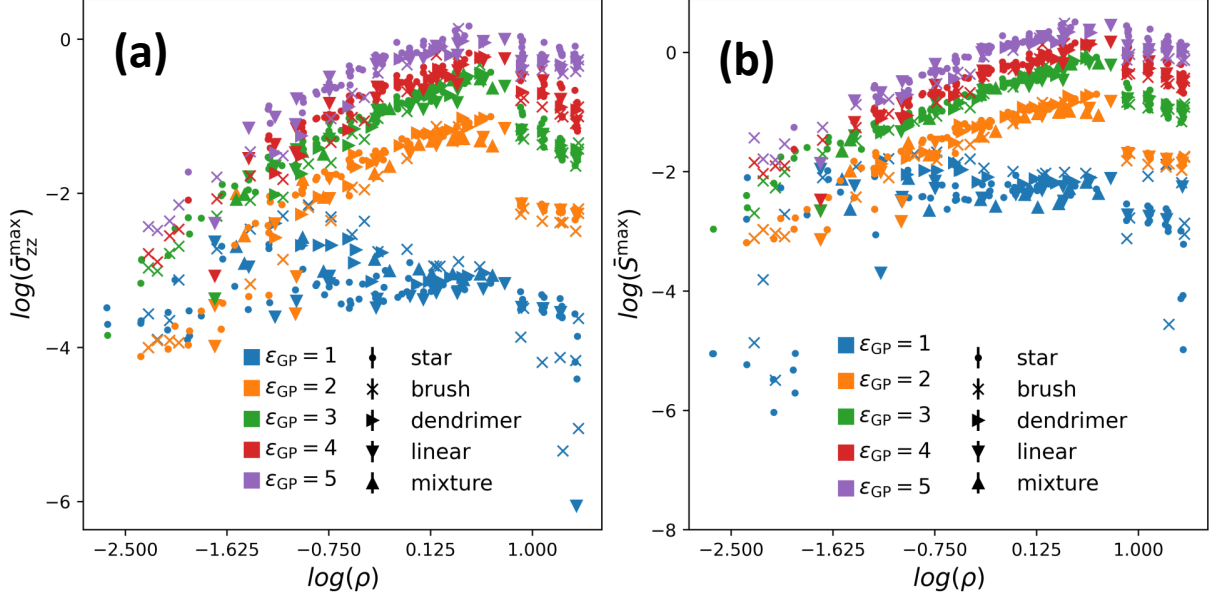


Figure 4: Log-log plot of (a) the stress at failure σ_{zz}^{\max} and (b) the maximum strain at failure \bar{s}^{\max} as a function of the surface density of gluing polymer ρ . Different colors represent different polymer affinities ϵ_{GP} while the shape of the data points represent polymer types (as in Fig.2). Note that all quantities are reported in reduced Lennard-Jones units.

curves. However, in our case the whole stress-strain curves, not only their integral, are also roughly the same.

In fact, what we observe is that the stress in the system shows the very same linear elastic behaviour for all gluing polymer architectures all the way up to the breaking point where the maximum stress is reached, at which point the stress falls abruptly to zero, see Fig.5 where we report a few representative cases. By visual inspection of the different MD trajectories, we can confirm that at the breaking point the gluing polymers are starting to be pulled out of the hydrogel network. While doing so, the stretched hydrogel returns to an unstressed state and breaking the interface at this point is irreversible. Fig. 1 is representative of this process, which is invariably detected in all our simulations. Based upon these observations, we take the state where the gluing polymer is being pulled out, but where the hydrogel network is otherwise relaxed, as the barrier state. In practice, the difference in free-energy between the barrier state and the initial equilibrium state (at zero strain and with the two hydrogels in contact) is relatively high. This is because to arrive to

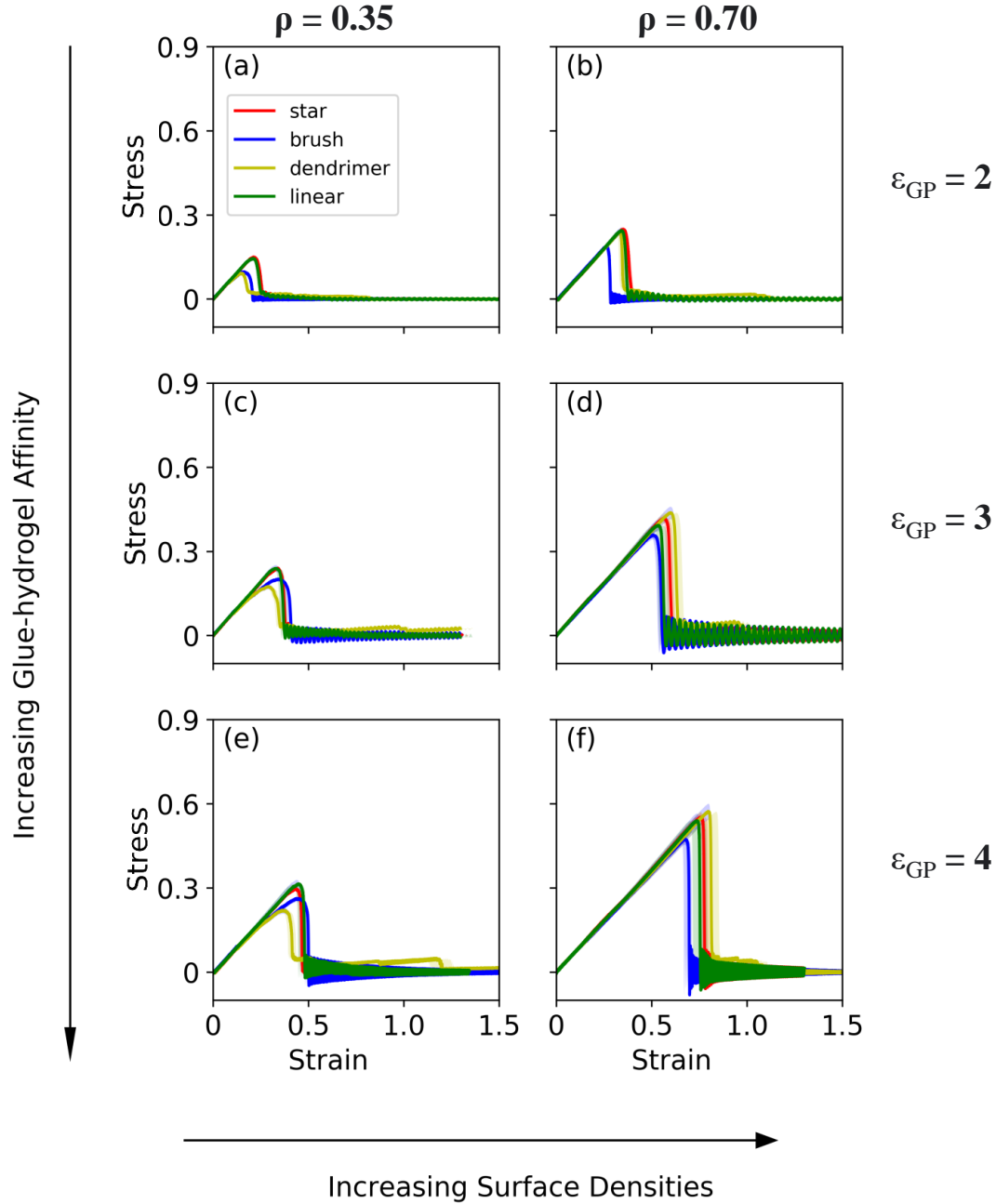


Figure 5: Representative stress-strain curves for the various architectures for three representative values of the glue-hydrogel affinity ϵ_{GP} , at two surface densities, (a) (c) (e) for $\rho = 0.35$ and (b) (d) (f) for $\rho = 0.70$. As it can be seen, the curves are very similar for all the different architectures, with an overlapping linear elastic behaviour up to the breaking, which only strongly depend on affinity. Note that all quantities are reported in reduced Lennard-Jones units.

the barrier state one requires both stretching the gluing polymer and pulling it out of the hydrogel, which in turn means breaking weak but multiple bonds. We thus expect breakage of

the two interfaces to be observable on the timescale of our simulations only when this barrier is largely compensated. In our case, the system accumulates elastic energy in the hydrogel network upon straining, lowering the difference in the free-energy with the barrier state. As the strain accumulates, this difference becomes of the order of a few $k_B T$ (the thermal energy in the system, where k_B is Boltzmann's constant), at which point the transition to the barrier state becomes kinetically accessible. In practice, this means that the strain energy measured via Eq. 4 should differ by only a few $k_B T$ from $\Delta F_{\text{barrier}}$. As initially argued, this strain energy corresponds to $\Delta F_{\text{adhesion}}$ under quasi-static conditions. We can thus use this fact to estimate an approximate value for $\Delta F_{\text{adhesion}}$ in our system, which we calculate by making two assumptions. First, each linear segment of the gluing polymer behaves as an ideal coil obeying Gaussian statistics.³¹ By linear segment here we mean a piece of polymer between two cross-linking points in any of the architectures reported in Table 1. Furthermore, we assume that at the breaking point by symmetry half of each polymer is in contact with the hydrogel network, whereas the other half will be fully stretched out of the hydrogel, see e.g. Fig. 1(d) for reference. For each segment, there are two contributions to the free-energy that needs to be considered. On the one side, Gaussian entropic elasticity will make each segment coil. On the other side, the affinity of the glue for the network, measured by ϵ_{GP} , would favour each segment to stretch to maximise contact with the polymer. Given these premises, the free-energy for a single linear segment as a function of the end to end distance x will be given by:

$$\Delta F(x) = -\epsilon_{GP}\mu x + \frac{3}{4} \frac{k_B T}{N_s a^2} x^2, \quad (5)$$

where μ is a proportionality constant, N_s the number of monomers, each of size a , in a linear segment. Assuming equilibrium, $\frac{\partial F}{\partial x} = 0$, would give for the equilibrium elongation x_e :

$$x_e = \frac{2}{3} \frac{\epsilon_{GP}}{k_B T} \mu N_s a^2, \quad (6)$$

and substituting the free-energy per glue segment in their equilibrium configuration gives:

$$F_e \equiv F(x = x_e) = -\frac{1}{3}\beta\mu^2\epsilon_{GP}^2N_s a^2, \quad (7)$$

which summing over all linear segments in the system results for the total free-energy at equilibrium:

$$F_{\text{equi}} = \sum_{i,s} -\frac{1}{3}\beta\mu^2\epsilon_{GP}^2N_iN_{i,s}a^2 = -\frac{1}{3}\beta\mu^2\epsilon_{GP}^2N_{\text{tot}}a^2 \quad (8)$$

Where the sum i is over all the N_i gluing polymers of architecture i and s is over the different linear segments in each gluing polymer type, each containing $N_{i,s}$ monomers, and thus N_{tot} is the total amount of glue monomers. Considering that, in the barrier state, by symmetry only half of the linear segments are interacting with the hydrogel (and in their equilibrium configuration) whereas the other half is pulled out and highly stretched, we have that $F_{\text{barrier}} = \frac{1}{2}F_{\text{equi}}$, and we thus obtain the final result:

$$\Delta F_{\text{adhesion}} \approx F_{\text{barrier}} - F_{\text{equi}} = \frac{1}{6}\beta\mu^2\epsilon_{GP}^2N_{\text{tot}}a^2. \quad (9)$$

Despite its simplicity, this model qualitatively capture a few observations. First, that $\Delta F_{\text{adhesion}}$ should only depend on the total amount of polymer glue inserted at the interface N_{tot} , but not on details of its architecture. In practice, this is a consequence of our assumption that every linear segment behaves independently from each other. For the same reason, we also obtain that the $\Delta F_{\text{adhesion}}$ increases linearly with the amount of glue at the interface, as we observe in Fig. 2. Finally, the model also predicts a super-linear dependence of $\Delta F_{\text{adhesion}}$ on the glue-polymer affinity, as measured by ϵ . However, it should be noted that this super-linearity is somewhat under-estimated by this model, which predicts $\Delta F_{\text{adhesion}} \propto \epsilon_{GP}^2$ behaviour vs the measured $\Delta F_{\text{adhesion}} \propto \epsilon_{GP}^{2.6}$. **Thus, in terms of a simple physical picture, the adhesive power of this types of glues in the low-concentration regime can be thought of as arising from the free-energy required to pull out of the hydrogel a partially stretched chain,**

this stretching occurs because of the balance between the polymeric entropy of the glue, which favours a relaxed coiled conformation, and the polymer affinity for the hydrogel, which instead tends to pull the polymer. Whereas we can expect each coil to act independently at low glue concentrations, and independence that allowed us to rationalise the gluing power with the simple model we have just presented, this approximation should eventually break down for higher values. In fact, we observe that $\Delta F_{\text{adhesion}}$ does not increase indefinitely with the amount of polymer glue but reaches a maximum and then declines. Even in this high-concentration region, the system response is still dominated by the affinity with the hydrogel. A very similar non-monotonic behaviour was also previously observed for hard nanoparticles-based glues,^{12,13} and similar arguments as those developed in those works can be used to rationalise this behaviour in the present system. The glue added at the interface can form bonds with the hydrogel network only up to a certain concentration where all the hydrogel chains are completely surrounded by the glue, at which point additional glue is prevented from entering in contact with it by excluded volume interactions. As the concentration of glue increases, excluded volume interactions also lead to an increase in the osmotic pressure which, together with the lack of attractive bonds with the hydrogel, push the additional glue to diffuse away from the interface and migrate towards the bulk of the hydrogel. In the bulk, the glue is stabilised by the presence of bare hydrogel with which to form bonds, but it does not act as a bridge between the two interfaces anymore.

This situation is clearly visible from the density distribution in the system reported in Fig. 6, where for glue concentrations are equal to 3 (see Fig. 6 (b)), one can observe that the glue diffuses away from the interface. The process of glue diffusion away from the interface is somewhat self-limiting. This is the case because as more glue migrate to the bulk, the osmotic pressure necessary to speed-up its diffusion away from the interface decreases and the remaining polymer remains confined there, where it is energetically stabilised by a higher hydrogel concentration compared to the bulk, with which it can form attractive interactions.¹³ This is likely the reason why, after a drop, adhesion does not drop all the

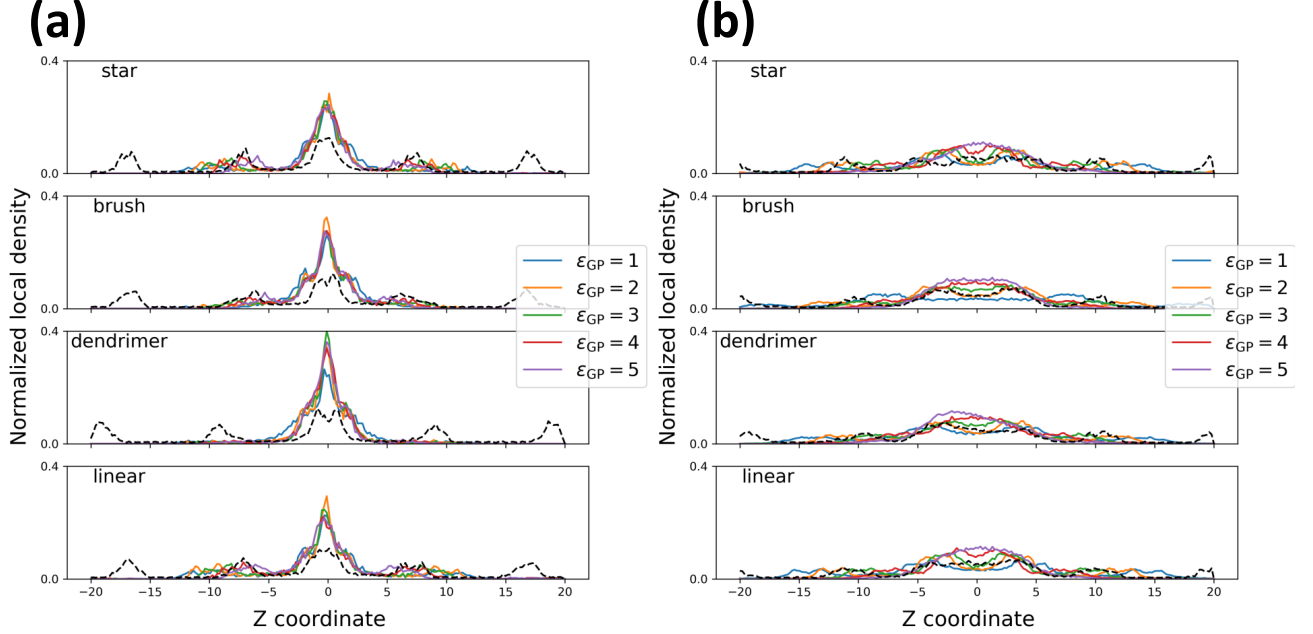


Figure 6: Normalized local number density of beads along the z axis for both the glue and the hydrogel, shown for different values of the total amount of glue deposited at the interface: (a) for $\rho = 1$ (b) for $\rho = 3$. These values of ρ have been chosen because they are above and below the loading at which the glue achieves maximum performance (higher $\Delta F_{\text{adhesion}}$). The (un-normalized) local density $\tilde{\rho}(z)$ is related to the total density ρ via $\int_{L_z} \tilde{\rho}(z) dz = \rho A = N_{\text{beads}}$. Colors represent different polymer glue-hydrogel affinities, as measured by the parameter ϵ_{GP} . The black-dotted curve represents the local density of the hydrogel, whereas continuous lines are used for the glue. Note that all quantities are reported in reduced Lennard-Jones units.

way down to zero. This view is also supported by calculating the bridging number $\langle B \rangle$, here defined as:

$$\langle B \rangle = \left\langle \frac{|E_1 + E_2|}{|E_1 - E_2| + 1} \right\rangle \quad (10)$$

where E_1 is the energy of interaction between the glue and the lower half of the gel, E_2 is the energy of interaction between the glue and the upper half of the gel and $\langle \cdot \rangle$ signifies an average over the equilibrium configurations of the system. The bridging number increases linearly with the amount of polymer if this sits right at the interface between the two hydrogels and is equally bound to them, whereas polymers that migrate to the bulk do not contribute to it. Note that, as for the density distribution of Fig 6, the bridging number

reported in Fig. 7 is calculated for each system at equilibrium just before straining. In our system the effective bridging increases with density, while it almost saturates at high values, approximately for $\rho > 1.5$. This occurs for all affinities except the highest one, possibly due to a lower diffusion coefficient which should be expected due to the stronger attractive interaction with the hydrogel.³² In fact, at the strongest affinity the high-loading regime also seems to differ, as instead of showing a clear plateau it seems that there is a stronger dispersion in all adhesion properties, something that is mirrored also in the bridging parameter.

We would now like to discuss our results in light of available experiments. Although we have not found any systematic study on the influence of glue architecture on adhesion in hydrogels, we can still compare to what have been observed for the case of glues based on linear polymers. Based on our simulations, we would expect adhesion should only depend linearly on the amount of glue at the interface, but not on how that density is achieved. This is indeed consistent with experimental observation on so-called tough adhesives,³ where they observe that, at constant polymer concentration, changing the molecular mass of the polymer used, i.e., the length of the chain, does not change the adhesion energy. In fact, the same experiments also show that, at constant molecular mass, the adhesion energy is linear in polymer concentration, which is what we observed. **In order to facilitate a meaningful comparison to future experiments, it is very important to understand what classes of polymer-based glues our results should apply to. In our investigations, we limited ourselves to the study of glues made of polymers whose mutual interaction are repulsive. This is because, as we previously argued when describing the system's interactions, most polymers used for hydrogel-gluing applications are hydrophilic and the effective, water-mediated interaction between chains is often repulsive in this case. In our system, the interface between the two hydrogels is kept together by the multiple and reversible weak bonds that each gluing chain forms with both of the two hydrogels, which constitute the only attractive interaction. This situation is very different from systems where strong attractive interactions are also present between**

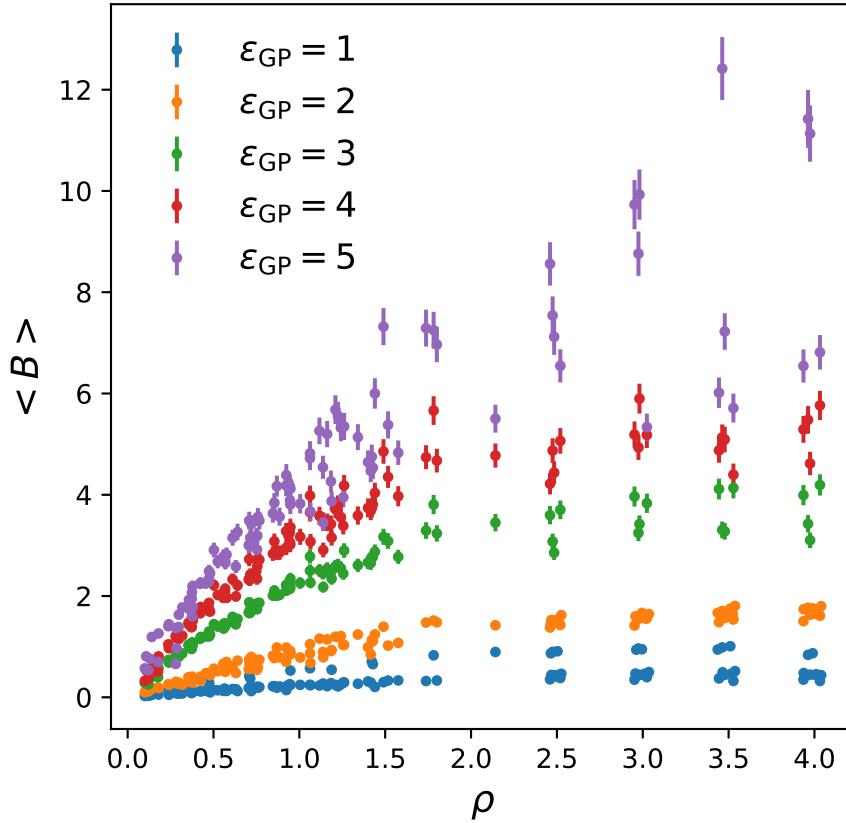


Figure 7: Bridging parameter (Eq. 10) versus glue surface density ρ , calculated for different glue polymer affinity ϵ_{GP} . The bridging parameter (see text for a definition) rapidly increases with increasing surface density up to $\rho \approx 1.5$, but then remains almost constant for all but the highest affinity considered. This effect is due to the glue migrating to the bulk above a certain surface density, where it does not act as bridge between the two hydrogels anymore, see also Fig.6. Note that all quantities are reported in reduced Lennard-Jones units.

the molecules that make up the glue, for example, when the glue is itself a highly viscous gel, often also irreversibly cross-linked to the two interfaces through covalent bonds, as in various recently proposed polysaccharides based glues.^{33–35} In this latter case, rupture at the interface can also occur from breaking of the bonds between the polymers that make up the glue itself, rather than those formed between the glue and the hydrogel substrate like in our case. When this occurs, rupture is said to be dominated by cohesive (glue-gel) rather than adhesive (glue-substrate) interactions.³⁶ When cohesive rupture is the dominant

mechanism, one would probably expect adhesion to benefit from stronger mutual attraction between the glue chains, e.g., through hydrogen bonding, although this does not seem to be always true.³⁷ In this case, the polymeric glue architecture might play an important role by hindering or facilitating internal bonds formation. These qualitative considerations show that because of the different dominant mechanisms leading to rupture, we cannot, and do not, expect our results to be also applicable to glues where cohesive rather than adhesive forces determine rupture. Instead, we expect our work to be instead relevant for the broad class of what de Gennes called “soft adhesives”,³⁸ where adhesion is controlled by the free-energy required to pull a polymer chain out of the substrate. In the future, it will be interesting to study the role of polymer architecture also in cohesion-dominated these systems, which could be done by adapting our computational model, e.g., modifying the interaction range of the Lennard-Jones potential and the ϵ_{GG} parameter to introduce and tune the glue-glue attraction strength.

Having specified the range of validity of our results, before we conclude we want to briefly discuss the significance of our results in terms of design principles for glues for hydrogels. First, because only the amount at the interface is important but not how this is achieved, any architecture could be used. For the same reason, there is no particular need to use relatively more complex synthetic techniques to reduce polydispersity, unlike what is required for many other applications where polymers are used to enhance mechanical properties. In this regard, however, there is a caveat. Although polydispersity is not crucial, the polymer lengths investigated here are all such that the polymer gyration radius is above the mesh size, and thus diffusion does not occur, unless a large concentration is achieved. As for the case of hard nanoparticles,¹³ for much smaller polymers diffusion away from the interface would still reduce the gluing power. Incidentally, this might explain some results observed in recent experiments by Yang *et al.*,³⁹ who used chitosan-based glues to bind together different porcine tissues, whose main structural component is a hydrogel. In these experiments, it was observed that increasing the polymerisation degree of the glue initially increased adhesion,

but for long enough polymer it becomes independent. Finally, the fact that the polymer architecture is not an important determinant for adhesion can be exploited to control other properties of the glue without the risk to affect adhesion. Consider for example the glue viscosity. For practical applications, it should be low enough so that depositing the glue via painting or through a syringe is easy. For linear polymers, decreasing polymer concentration in a solution decreases its viscosity, but as we have seen it would also decrease its gluing power. However, because the viscosity of star-like or bottle brush polymers at the same concentration is lower than for linear ones, by using these branched architectures one can use more concentrated solutions, improving adhesion while keeping the viscosity in the application-relevant regime.

Conclusion

In this paper, we have investigated via coarse-grained modelling and MD simulations the effect of polymer architecture when a polymer solution is used as a glue between two hydrogels. We have observed that the adhesion energy is super-linear in the affinity and linear in the total amount of polymer at the interface, but is roughly independent on the polymer architecture. Compared to glues based on solutions of hard nanoparticles, polymer-based glues might provide specific advantages in terms of robustness because they never act as anti-adhesives, regardless of their concentration or their affinity for the hydrogel.

Our results should provide useful guidance for the technologists working on the development of polymer-based bio-adhesives. In practice, the architecture-independent behaviour shown in our simulations means that the polymer architecture can be used as a way to tune other properties necessary for their application, for example, the viscosity of the gluing solution, without worrying about how this would affect adhesion. Moreover, our results also mean that polydispersity should not strongly affect the efficacy of the glue, allowing one to use cheaper and faster synthesis techniques. We also notice in general that polymers can be

synthesised in bulk quantity and with a large variety of chemistry more difficult to access with inorganic nanoparticles at a fraction of their cost, which would also increase their mass adoption for this kind of biomedical applications. Finally, it is necessary to point out that within a coarse-grained model, chemistry dependent effects can only be described qualitatively. Thus, we are unable to discuss issues such as bio-compatibility. We notice, however, that FDA-approved polymers as bio-adhesives already exist and their performance can then be controlled considering different potential architectures, the primary goal of our paper. Given these premises, we would welcome experiments aiming at fully validating the simulations presented here, and we hope the results presented in this paper will spur further research into the development of polymer-based glues for hydrogels and biological tissues.

Supporting Information Available

[Entire simulation protocol and details](#)

Acknowledgement

The authors acknowledge the China Scholarship Council for funding via a PhD scholarship, and access to computation resources from the Thomas Young Centre London and the Imperial College High-Performance Computing Service.

References

- (1) Kinloch, A. J. *Adhesion and Adhesives: Science and Technology*; Springer Science & Business Media, 2012.
- (2) Rose, S.; PrevotEAU, A.; ElzIere, P.; Hourdet, D.; Marcellan, A.; Leibler, L. Nanoparticle Solutions as Adhesives for Gels and Biological Tissues. *Nature* **2014**, *505*, 382.

- (3) Li, J.; Celiz, A.; Yang, J.; Yang, Q.; Wamala, I.; Whyte, W.; Seo, B.; Vasilyev, N.; Vlassak, J.; Suo, Z. Tough Adhesives for Diverse Wet Surfaces. *Science* **2017**, *357*, 378–381.
- (4) Chen, X.; Yuk, H.; Wu, J.; Nabzdyk, C. S.; Zhao, X. Instant Tough Bioadhesive with Triggerable Benign Detachment. *Proceedings of the National Academy of Sciences of the United States of America* **2020**, *117*, 15497–15503.
- (5) Appel, E. A.; Scherman, O. A. Gluing gels: A Nanoparticle Solution. *Nature materials* **2014**, *13*, 231–232.
- (6) Yang, J.; Bai, R.; Chen, B.; Suo, Z. Hydrogel Adhesion: A Supramolecular Synergy of Chemistry, Topology, and Mechanics. *Advanced Functional Materials* **2020**, *30*, 1901693.
- (7) Kopeček, J.; Yang, J. Hydrogels as Smart Biomaterials. *Polymer international* **2007**, *56*, 1078–1098.
- (8) Geckil, H.; Xu, F.; Zhang, X.; Moon, S.; Demirci, U. Engineering Hydrogels as Extracellular Matrix Mimics. *Nanomedicine* **2010**, *5*, 469–484.
- (9) Wirthl, D.; Pichler, R.; Drack, M.; Kettlguber, G.; Moser, R.; Gerstmayr, R.; Hartmann, F.; Bradt, E.; Kaltseis, R.; Siket, C. M. Instant Tough Bonding of Hydrogels for Soft Machines and Electronics. *Science advances* **2017**, *3*, e1700053.
- (10) Nam, S.; Mooney, D. Polymeric Tissue Adhesives. *Chemical Reviews* **2021**, DOI: 10.1021/acs.chemrev.0c00798, in press.
- (11) Lang, N.; Pereira, M. J.; Lee, Y.; Friehs, I.; Vasilyev, N. V.; Feins, E. N.; Ablasser, K.; O’Cearbhaill, E. D.; Xu, C.; Fabozzo, A. A Blood-resistant Surgical Glue for Minimally Invasive Repair of Vessels and Heart Defects. *Science translational medicine* **2014**, *6*, 218ra6–218ra6.

- (12) Molinari, N.; Angioletti-Uberti, S. Nanoparticle Organization Controls Their Potency as Universal Glues for Gels. *Nano letters* **2018**, *18*, 3530–3537.
- (13) Molinari, N.; Jung, G.; Angioletti-Uberti, S. Designing Nanoparticles as Glues for Hydrogels: Insights from a Microscopic Model. *Macromolecules* **2021**, *54*, 1992–2000.
- (14) Likos, C. N.; Löwen, H.; Watzlawek, M.; Abbas, B.; Jucknischke, O.; Allgaier, J.; Richter, D. Star Polymers Viewed as Ultrasoft Colloidal Particles. *Physical Review Letters* **1998**, *80*, 4450–4453.
- (15) Arno, M. C.; Inam, M.; Weems, A. C.; Li, Z.; Binch, A. L.; Platt, C. I.; Richardson, S. M.; Hoyland, J. A.; Dove, A. P.; O’Reilly, R. K. Exploiting the Role of Nanoparticle Shape in Enhancing Hydrogel Adhesive and Mechanical Properties. *Nature Communications* **2020**, *11*, 1420.
- (16) Daoud, M.; Cotton, J. P. Star Shaped Polymers: a Model for the Conformation and Its Concentration Dependence. *Journal de physique Paris* **1982**, *43*, 531–538.
- (17) Mladek, B. M.; Gottwald, D.; Kahl, G.; Neumann, M.; Likos, C. N. Formation of Polymorphic Cluster Phases for a Class of Models of Purely Repulsive Soft Spheres. *Physical Review Letters* **2006**, *96*, 3–6.
- (18) Kim, W. K.; Moncho-Jordá, A.; Roa, R.; Kanduc, M.; Dzubiella, J. Cosolute Partitioning in Polymer Networks: Effects of Flexibility and Volume Transitions. *Macromolecules* **2017**, *50*, 6227–6237.
- (19) Marrink, S. J.; Risselada, H. J.; Yefimov, S.; Tieleman, D. P.; De Vries, A. H. The MARTINI force field: coarse grained model for biomolecular simulations. *The journal of physical chemistry B* **2007**, *111*, 7812–7824.
- (20) Cornell, W. D.; Cieplak, P.; Bayly, C. I.; Gould, I. R.; Merz, K. M.; Ferguson, D. M.; Spellmeyer, D. C.; Fox, T.; Caldwell, J. W.; Kollman, P. A. A second generation force

- field for the simulation of proteins, nucleic acids, and organic molecules. *Journal of the American Chemical Society* **1995**, *117*, 5179–5197.
- (21) Angioletti-Uberti, S. Theory, simulations and the design of functionalized nanoparticles for biomedical applications: A Soft Matter Perspective. *npj Computational Materials* **2017**, *3*, 48.
- (22) Wang, X.; Ramírez-Hinestrosa, S.; Dobnikar, J.; Frenkel, D. The Lennard-Jones potential: When (not) to use it. *Physical Chemistry Chemical Physics* **2020**, *22*, 10624–10633.
- (23) van Oss, C. J. Long-range and short-range mechanisms of hydrophobic attraction and hydrophilic repulsion in specific and aspecific interactions. *Journal of Molecular Recognition* **2003**, *16*, 177–190.
- (24) Kanduč, M.; Netz, R. R. From hydration repulsion to dry adhesion between asymmetric hydrophilic and hydrophobic surfaces. *Proceedings of the National Academy of Sciences* **2015**, *112*, 12338–12343.
- (25) Stukowski, A. Visualization and Analysis of Atomistic Simulation Data with OVITO the Open Visualization Tool. *Modelling and Simulations in Materials Science and Engineering* **2010**, *18*.
- (26) Martyna, G. J.; Tobias, D. J.; Klein, M. L. Constant Pressure Molecular Dynamics Algorithms. *The Journal of Chemical Physics* **1994**, *101*, 4177–4189.
- (27) Glaser, J.; Nguyen, T. D.; Anderson, J. A.; Lui, P.; Spiga, F.; Millan, J. A.; Morse, D. C.; Glotzer, S. C. Strong Scaling of General-purpose Molecular Dynamics Simulations on GPUs. *Computer Physics Communications* **2015**, *192*, 97–107.
- (28) Anderson, J. A.; Lorenz, C. D.; Travesset, A. General Purpose Molecular Dynamics

- Simulations Fully Implemented on Graphics Processing Units. *Journal of Computational Physics* **2008**, *227*, 5342–5359.
- (29) Cao, Z.; Dobrynin, A. V. Nanoparticles as Adhesives for Soft Polymeric Materials. *Macromolecules* **2016**, *49*, 3586–3592.
- (30) Sayko, R.; Cao, Z.; Liang, H.; Dobrynin, A. V. Gluing Interfaces with Soft Nanoparticles. *Langmuir* **2019**, *35*, 7277–7284.
- (31) Rubinstein, M.; Colby, R. H. *Polymer physics*; Oxford university press New York, 2003; Vol. 23.
- (32) Kim, W. K.; Chudoba, R.; Milster, S.; Roa, R.; Kanduč, M.; Dzubiella, J. Tuning the Selective Permeability of Polydisperse Polymer Networks. *Soft Matter* **2020**, *16*, 8144–8154.
- (33) Tang, X.; Gu, X.; Wang, Y.; Chen, X.; Ling, J.; Yang, Y. Stable antibacterial polysaccharide-based hydrogels as tissue adhesives for wound healing. *RSC Advances* **2020**, *10*, 17280–17287.
- (34) Cha, C.; Antoniadou, E.; Lee, M.; Jeong, J. H.; Ahmed, W. W.; Saif, T. A.; Boppart, S. A.; Kong, H. Tailoring hydrogel adhesion to polydimethylsiloxane substrates using polysaccharide glue. *Angewandte Chemie International Edition* **2013**, *52*, 6949–6952.
- (35) Patel, A. K.; Mathias, J.-D.; Michaud, P. Polysaccharides as adhesives. *Reviews of Adhesion and Adhesives* **2013**, *1*, 312–345.
- (36) Lee, B. P.; Messersmith, P. B.; Israelachvili, J. N.; Waite, J. H. Mussel-inspired adhesives and coatings. *Annual review of materials research* **2011**, *41*, 99–132.
- (37) Serrero, A.; Trombotto, S.; Bayon, Y.; Gravagna, P.; Montanari, S.; David, L.

Polysaccharide-based adhesive for biomedical applications: correlation between rheological behavior and adhesion. *Biomacromolecules* **2011**, *12*, 1556–1566.

(38) de Gennes, P.-G. Soft adhesives. *Langmuir* **1996**, *12*, 4497–4500.

(39) Yang, J.; Bai, R.; Suo, Z. Topological Adhesion of Wet Materials. *Advanced Materials* **2018**, *30*, 1800671.

Graphical TOC Entry

